ISSN 1027-4510, Journal of Surface Investigation: X-ray, Synchrotron and Neutron Techniques, 2019, Vol. 13, No. 3, pp. 555–561. © Pleiades Publishing, Ltd., 2019.
Russian Text © The Author(s), 2019, published in Poverkhnost', 2019, No. 6, pp. 101–108.

Changes in the Structure and Microhardness of Rapidly Solidified Foils of Aluminum Alloy 1421 during Their Annealing

V. G. Shepelevich[a], I. A. Bushkevich[a, *], E. Wendler[b], and I. I. Tashlykova-Bushkevich[c, **]

[a] *Belarusian State University, Minsk, 220050 Belarus*
[b] *Schiller University, Jena, 07743 Germany*
[c] *Belarusian State University of Informatics and Radioelectronics, Minsk, 220013 Belarus*
**e-mail: uyluana@gmail.com*
***e-mail: iya.itb@bsuir.by*

Received June 26, 2018; revised October 12, 2018; accepted October 12, 2018

Abstract—In this work, the relationship between the microstructure and microhardness of Al–Mg–Li–Zr–Sc alloy (1421 Al) prepared by ultrafast quenching from the melt has been studied. The following methods are used in studying the rapidly solidified (RS) alloy: scanning electron microscopy integrated with energy dispersive X-ray microanalysis, the method of nuclear reaction analysis, and the measurement of microhardness changes during isochronal annealing. The intercept method is applied to determine the size of secondary phases, their volume fraction, and the specific surface area of the interface boundaries in the samples. It is established that the as-quenched rapidly solidified alloy foils are composed of an aluminum-based supersaturated solid solution. It is found that lithium, the content of which reaches 9.0 at %, is unevenly distributed over the subsurface region of foils. After annealing at 300°C, precipitates of (Sc, Zr)-containing phase are detected in the structure of foils in addition to magnesium-containing phases. Nonmonotonic changes in the microhardness are observed during isochronal annealing of the foils in the temperature ranges of 50–100°C, 150–210°C, 230–340°C, which are associated with the precipitation of metastable and stable phases. It is found that heating of the alloy foils to 340°C leads to an increase in the microhardness by 23%, and a sharp decrease in the microhardness takes place at temperatures above 400°C.

Keywords: rapid solidification, Al–Mg–Li–Zr–Sc alloy, phase composition, microhardness
DOI: 10.1134/S1027451019030327

INTRODUCTION

The stability of properties during operation is one of the most important requirements for aeronautical engineering materials. Aluminium alloys with an Mg content of less than 7 wt % possess properties that are nearly the same in the annealed, quenched, and aged states. The supersaturated solid solution of magnesium in aluminum is characterized by a relatively high strength and good corrosion resistance together with high plasticity [1]. The effect of strengthening in alloys of the Al–Mg system doped with lithium was discovered in 1965 by academician I.N. Frindlyander [2]. It should be noted for Al–Mg–Li alloys that their strength is comparable to the strength of other aluminium alloys widely used in aviation. On account of the addition of lithium, the alloy density decreases and the elastic modulus increases. At the same time, the specifics of the heat treatment of alloys of the Al–Mg–Li system are associated with the presence of the reinforcing δ' phase (Al_3Li), the decomposition morphology of the supersaturated α-solid solution, the nature of the precipitated additional phases, and their volume-fraction ratio [3]. However, Al–Mg–Li alloys in the coarse-grained state demonstrate limited technological plasticity and low service properties due to strain localization.

Currently, most aluminum alloys are doped with rare-earth and transition-metal additives to enhance their strength and corrosion properties. The effect of the addition of Sc ensures higher strength characteristics in alloys of the Al–Mg system in comparison with the addition of Mn and Zr, which are frequently used as anti-crystallizing agents for aluminium [4–6]. A high radiation resistance of Al–Mg alloys with scandium is reported in [7–9]. The use of Sc together with Zr is also considered to be promising. It is known that only 0.1–0.2 wt % of scandium and zirconium gives rise to a three-fold increase in the strength of aluminium [10]. Zirconium added together with scandium not only replaces a part of expensive scandium, but additionally gives a high strength, weldability, and corrosion resistance to aluminium-based alloys [11], which is especially important in aeronautical engineering.

A large number of publications are devoted to studying the microstructure, phase composition, and mechanical properties of cast samples of industrial Al–Mg–Li–Zr–Sc alloy of the brand 1421 [12–14]. However, modern methods for structural modification are actively sought to improve the properties of this alloy, namely, methods based on treatment with pulsed laser radiation [15] and methods of severe plastic deformation (for example, equal channel angular extrusion (ECAE) [16–18]) are used. Therefore, it can be concluded that the use of methods of ultrafast quenching from the melt (UFQM) [19] is also of scientific and practical interest for improving the physicomechanical properties of alloy 1421 and the development of novel aluminium alloys for operation at elevated temperatures. With UFQM, significant dispersion of the structural components of the material occurs, including the refinement of grains, the particle sizes of secondary phases decrease, anomalously supersaturated solid solutions are produced, and metastable intermediate phases are formed.

In this study, the morphology, and the elemental and phase compositions of alloy 1421 prepared by rapid crystallization from the melt are determined, as well as changes in the microstructure and microhardness of rapidly solidified (RS) foils of alloy 1421 upon annealing are studied. For this purpose, the method of scanning electron microscopy (SEM) combined with energy dispersive X-ray microanalysis (EDX) and the method of nuclear reaction analysis (NRA) are used. The parameters of the microstructure of alloys are determined by the method of random secants. The Vickers microhardness values of the as-quenched and annealed samples are measured.

EXPERIMENTAL

The studied foils of industrial alloy 1421 with an elemental composition that includes Al with additions of 5.5 wt % Mg, 2.2 wt % Li, 0.12 wt % Zr, and 0.2 wt % Sc were prepared by ultrafast quenching from the liquid phase by the method of unilateral cooling. A thin layer of the melt was crystallized on the inner surface of a copper cylinder with a diameter of 20 cm, which was rotated with a frequency of 1500 rpm. The cooling rate of the melt was about 10^6 K/s [20]. The thickness of the studied foils was 40–80 μm. For comparison, a bulk sample in the shape of a parallelepiped, which was cut from cast homogeneous alloy 1421 and subjected to isothermal annealing at 300°C for 5 h, was used. To measure the size of secondary phase precipitates, their volume fraction, V, and the specific surface area, S, of the interface boundaries in the samples, the intercept method [21] with a relative error of 8% was used.

The morphology and elemental composition of the cross sections of as-quenched foil samples annealed at 300°C for 1 h, as well as a cast homogeneous sample, were studied using a LEO1455VP scanning electron microscope with an HKL CHANNEL5 attachment. The measurements were carried out with an acceleration voltage of 20 kV in the mode of detection of backscattered electrons. The diameter of the X-ray generation region was about 3 μm.

The lithium content in the subsurface region of both foil sides, i.e., surface A which is in contact with the substrate (copper cylinder) during quenching and the opposite surface, B, which is in contact with air, was investigated by the NRA method using the ^{7}Li(p, α)^{4}He nuclear reaction with an energy of protons of 1.4 MeV the backscattering angle θ was 170°. These measurements were performed on a JULIA (Jena University Laboratory for Ion Acceleration) Tandentron accelerator (3 MeV) with a detector resolution of 15 keV. The concentration of lithium in the foils was determined with an accuracy of 11% by the NRA method using the standard NRA spectrum obtained under the same conditions and geometry, as in the present experiments, from a sample of lithium niobate ($LiNbO_3$) containing 20.0 at % Li [22].

The microhardness, H_μ, was measured using a PMT-3 tester with a load of 50 g and an exposure time of 60 s. The dependence of the H_μ value of the foils on the exposure time at room temperature and under conditions of isochronal annealing was studied. Isochronal annealing of the foils was implemented from room temperature to 450°C in intervals of 20°C and 30 min exposures at each temperature. The error in the microhardness measurements was 4%.

RESULTS AND DISCUSSION

The SEM and EDX methods showed that there are no inclusions of secondary phases in the volume of the as-quenched foils of alloy 1421 (Fig. 1a), i.e., the RS alloy is composed of supersaturated α-solid solution. Figure 1c shows the microstructure of cast alloy 1421 imaged with backscattered electrons. The results of local analysis of the elemental composition of phases in the cast sample are shown in Table 1. Data on the content of lithium in the sample are not given in Table 1 because of limitations of the EDX method when elements are lighter than beryllium [23].

The lithium contents in both surfaces of the foil of alloy 1421 were determined using a proton beam by means of resonance in the ^{7}Li(p, α)^{4}He reaction. Since the energy of the emitted α-particles (products of this nuclear reaction) far exceeds the energy of protons incident on the sample, this makes it possible to detect lithium in the foil without noise. The NRA signal from lithium is observed in channel no. 419 (Fig. 2a). For comparison, the NRA spectrum of a standard $LiNbO_3$ sample with a Li concentration of 20.0 at % [22] is also given in Fig. 2b. As can be seen from Fig. 2, the experimental and standard NRA spectra are similar. This allows one to estimate that the lithium content in the foil subsurface layers is approximately 9.0 at %, which on 11% exceeds the calculated lithium content in

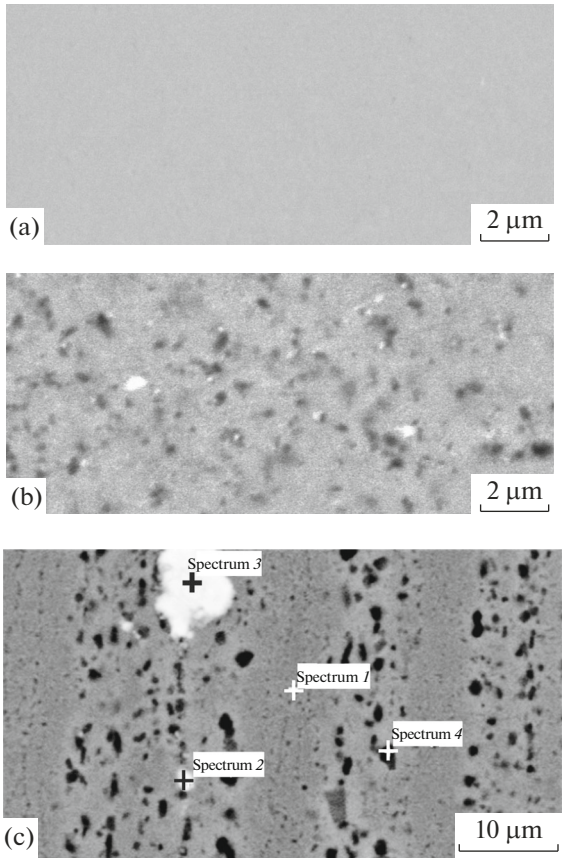

Fig. 1. SEM images of the cross sections of (a) an as-quenched foil, (b) a foil annealed at 300°C, and (c) a cast sample of alloy 1421. The numbers designate regions, in which the chemical composition of the sample was determined by the EDX method.

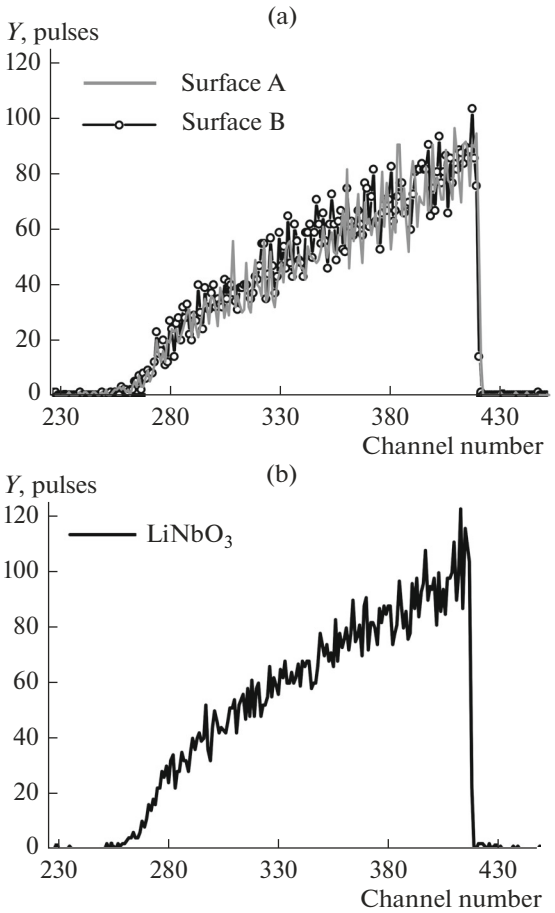

Fig. 2. NRA spectra obtained from (a) surfaces A and B of the foil of alloy 1421 and (b) the standard lithium niobate ($LiNbO_3$) sample under bombardment of targets with protons of 1.4 MeV at an angle of θ.

alloy 1421. The observed fact of enriching the surface of the foils with lithium indicates its nonuniform distribution over the foil thickness. Apparently, this effect is caused by the fact that the surface of foils and grain boundaries serve as sinks for the "quenching vacancies–atoms of dissolved elements" complexes [24, 25] and was observed by us earlier in RS binary aluminium alloys with Ti, V, Cr, Mn, Fe, Co, Ni, Cu, Zn, Ge, Sb [26, 27]. Li atoms (which is an active easily oxidizing element) diffusing from the bulk of the samples to the surface react with oxygen and form the lithium compound Li_2CO_3. It was reported in [28, 29] that the oxide film on the surface of alloy 1421 prepared by the ECAE method mainly consists of Li_2CO_3 and MgO after laser pulse treatment, as in the case of samples of alloy 1420 (close in composition to alloy 1421) annealed at a temperature of 450°C.

A solid solution of aluminium with precipitates of intermetallic phases was observed in the study of the microstructure of the cast sample of alloy 1421 (see Table 1 and region *1* in Fig. 1c). Along with the precipitates of magnesium-containing phases in the form of dark particles, light unevenly distributed inclusions containing Mg, Al, Sc, and Zr are detected (regions *2* and *3* in Table 1), which points to the formation of the $Al_3(Sc, Zr)$ compound [30, 31], which also may contain Li atoms [32]. In later publications [18, 33, 34], the existence of a more complex phase of the Al(Mg, Sc, Zr, Li)$_x$ composition instead of the above phase is

Table 1. Local chemical composition of phases in the structure of a homogenized ingot of alloy 1421

Analyzed region	Elemental composition, wt % (at %)				
	O	Mg	Al	Sc	Zr
1	0.80 (1.34)	5.40 (5.92)	93.80 (92.74)	–	–
2	1.02 (1.80)	3.31 (3.84)	83.35 (88.16)	7.19 (4.59)	5.13 (1.61)
3	0.99 (1.96)	1.37 (1.78)	68.81 (80.42)	16.52 (11.59)	12.31 (4.26)
4	1.27 (2.10)	5.27 (5.76)	93.47 (92.13)	–	–

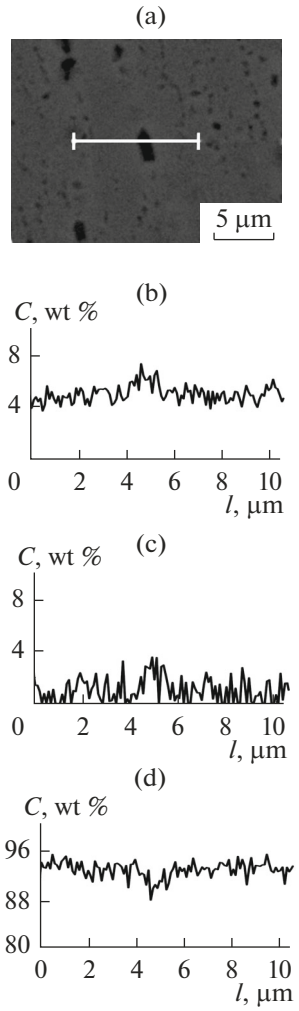

Fig. 3. (a) SEM image of a cast sample of alloy 1421 and (b–d) the results of EDX analysis performed along the specified scanning line for Mg, O and Al contents, respectively.

established in samples of alloy 1421 prepared in a nonequilibrium state after ECAE. On account of the presence of scandium and zirconium atoms, particles of this phase can be stable and retained until high temperatures are reached.

The size of dark precipitates (Fig. 1c) is smaller than the X-ray generation region in EDX, which makes it difficult to determine the local chemical composition of the magnesium-containing phases. The measurements showed that the data obtained for corresponding region *4* of the sample and given in Table 1 are close to the values determined in region *1* (Fig. 1c). To clarify the chemical composition of the dark precipitates, the distribution of elements in the cast sample along the line was additionally scanned. The results given in Fig. 3 showed that the magnesium content in the large dark precipitates is about 6.0 wt % (6.1 at %) on average. Therefore, it can be concluded that the precipitates of this second phase correspond to the β phase (Al_3Mg_2) [1, 35]. At the same time, it should be noted that particles of the S_1 phase (Al_2MgLi), which precipitates in alloys of the Al–Mg–Li system like the β phase after exposure to a temperature of 300°C [36], can also be present in the cast sample alloy 1421 after homogenization. However, the β and S_1 phases cannot be distinguished by the SEM and EDX methods within this study; therefore, they will hereinafter be referred to as "magnesium-containing phases".

The precipitates of magnesium-containing phases, as well as the particles of (Sc, Zr)-containing phase with mean chord lengths of 0.18 and 0.20 μm, respectively, are revealed in the microstructure of the RS foils after their annealing at a temperature of 300°C (see Fig. 1c). Histograms in the distribution of random secants on the sections of intermetallic particles in the cross sections of the annealed foils over the size groups of chords are given in Fig. 4a. The main part of the chords for the dark and light precipitates falls into the first size group extending from 0.05 to 0.15 μm and the second size group extending from 0.15 to 0.25 μm, respectively. The precipitates of these phases are finely dispersed unlike the precipitates of secondary phases in the cast sample (Figs. 4b and 4c), in which the main part of chords on the sections of the dark and light precipitates falls into the size group extending from 0.3 to 0.5 μm and the size group extending from 0.5 to 1.5 μm, respectively.

It is found that the total volume fractions of precipitates of magnesium-containing phases in the annealed foil and homogenized bulk sample are approximately the same and equal 3.4 and 2.9 vol %, respectively. However, the specific surface area of interface boundaries in the RS alloy increases after annealing from 0.21 μm^{-1} in the cast sample to 0.51 μm^{-1} in the annealed foil as a result of the dispersed particle size of the dark precipitates. It is found for the (Sc, Zr)-containing phase that the volume fraction of light precipitates increases (0.35 vol % in the cast sample vs. 0.46 vol % in the annealed foil). The specific surface areas of the interface boundaries of the light precipitates in the cast sample and annealed foil are 0.08 and 0.40 μm^{-1}, respectively, i.e., the S value increases 5 times with a decrease in the particle size upon an increase in the V value by 30% in the foils after annealing in comparison with the cast sample.

The dependence of the microhardness of RS alloy 1421 on the time of aging at room temperature is given in Fig. 5a. It is found that the microhardness of the as-quenched foils is 965 MPa, which is 35% higher than for the cast samples with $H_\mu = 627$ MPa. It was determined that the aging of foils for 5 h leads to an increase in the microhardness by 19%. Afterward, the H_μ value of the samples remains almost unchanged. This dependence of the microhardness on the exposure time can be attributed to the creation of high concentrations of vacancies upon ultrafast quenching from

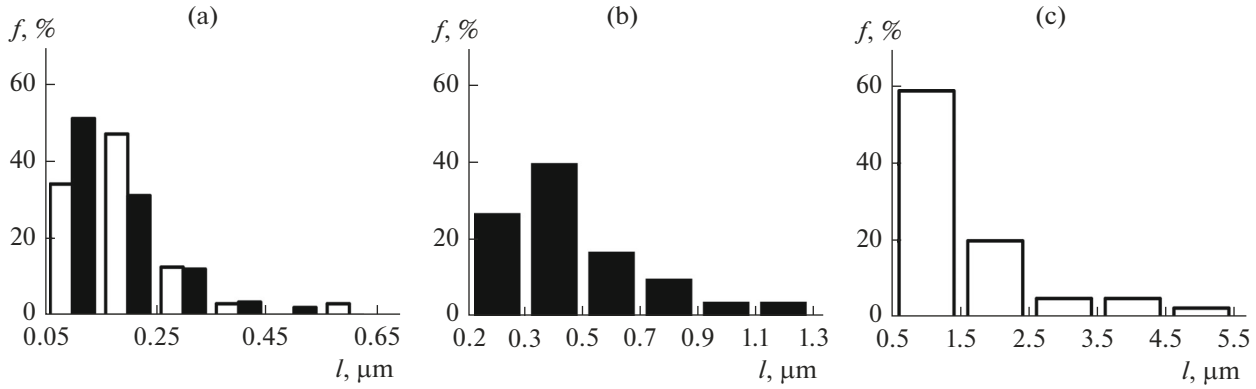

Fig. 4. Distribution of section chords of precipitates of (■) magnesium-containing and (□) (Sc, Zr)-containing phases over size groups in the (a) annealed foil and (b, c) cast sample of alloy 1421.

the liquid phase. Vacancies actively diffuse at room temperature and form clusters with doping elements, thereby increasing the microhardness upon the aging of foils.

The dependence of the microhardness of foils of alloy 1421 on the temperature of isochronal annealing is given in Fig. 5b. A nonmonotonic change of the H_μ value with an increase in the heating temperature is observed. An increase in the microhardness is observed in the temperature ranges of 50–100°C, 150–210°C, and 230–340°C, which is followed by a decrease at higher temperatures. The complex behavior of the H_μ value of foils during isochronal annealing indicates that structural and phase transformations take place in the RS alloy.

In the process of annealing RS alloy 1421, a low-temperature maximum of the microhardness is observed in the initial stage at a temperature of approximately 100°C (Fig. 5b). This initial increase in the H_μ value of the foils may be associated with the formation of clusters of doping elements, which involves vacancies that are generated in the process of foil preparation. A decrease in the microhardness upon a further increase in the annealing temperature up to 150°C can be explained by the decay of these clusters [37]. We previously reported a similar effect of the influence of clusters of doping elements on the microhardness during annealing for RS foils of alloy AMg6 of the Al–Mg–Mn system [38] and alloy 6061 of the Al–Mg–Si system [39].

The next stage of microhardness changes in the foils of alloy 1421 is explained by the precipitation of lithium-containing intermetallic phases. As in the case of RS powders of Al–Li–Mg–Zr alloys [40], the amount of precipitates of the metastable δ' phase (Al_3Li) increases in the annealing temperature range of 110–190°C. Further annealing of the powders gives rise to dissolution of the δ' phase at 230°C. Moreover, it should be noted that the reinforcing $S_1(Al_2MgLi)$ phase appears in alloy 1421 in addition to the δ' phase [40, 41], the precipitates of which show the highest density in the temperature range of 270–370°C.

An increase in the microhardness in the range of 260–340°C and a subsequent plateau in the curve of

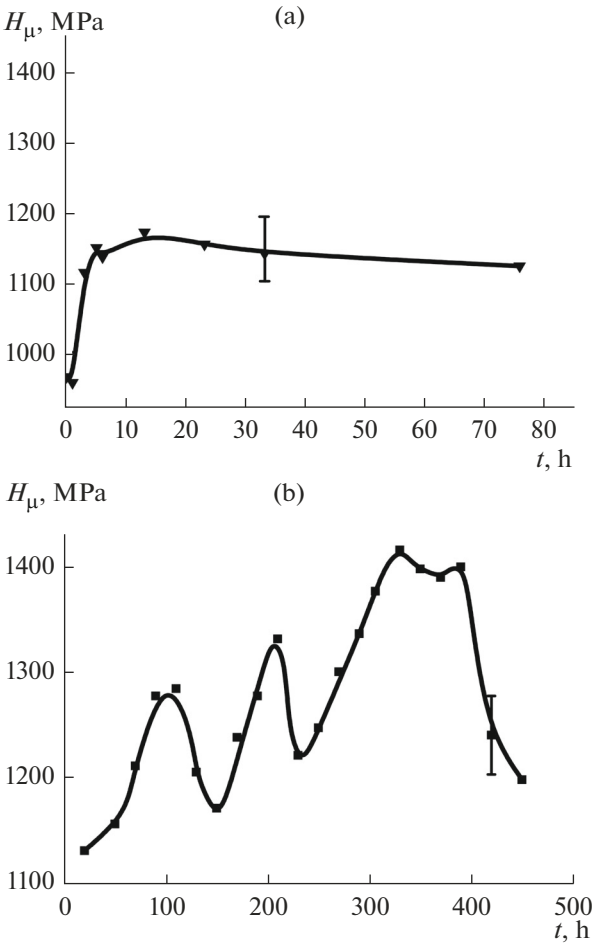

Fig. 5. Dependence of the microhardness of the foils on the exposure time (a) at room temperature and (b) under conditions of isochronal annealing.

the dependence of the microhardness on the isochronal annealing temperature that extends up to 400°C is explained by the combined action of the S_1 and Al(Mg, Sc, Zr, Li)$_x$ phases, the finely dispersed precipitates of which are found in the foils annealed at 300°C (Fig. 1b). As is known, the highest density of precipitates of this (Sc, Zr)-containing phase in ultrafine grained samples of alloy 1421 prepared by ECAE is observed in the range of 340–410°C [34]. Apparently, a significant decrease in the microhardness of the alloy foils when they are heated above 400°C is caused by the processes of the consolidation of intermetallic precipitates, which are followed by the processes of their dissolution and recrystallization [42] accompanied by particle coarsening. In addition, it should be noted that the processes of precipitation of the metastable β' phase (Mg_5Al_8) begin at 47°C and proceed to a temperature of 277°C [35, 43]. The stable β phase is formed either from the β' phase at annealing temperatures of about 200°C or directly from the supersaturated solid solution at temperatures above 277°C up to 375–400°C (Fig. 1a). Furthermore, these phases do not substantially contribute, according to the results of this study, to the microhardness changes during annealing of the foils of alloy 1421 unlike the RS foils of the Al–Mg–Ni and Al–Mg–Fe alloys [38, 39], as well as the foils of the Al–Mg alloy after intense torsional plastic deformation [44–46]. For these magnesium-containing aluminium alloys, an increase in the microhardness is observed in the annealing temperature range of 160–250°C.

Currently, alloy 1421 has not been investigated in foreign laboratories, since its analogues have a different composition in other countries. On the one hand, this is explained by the difficulty in the melting and casting of alloys of the Al–Mg–Li system with a high degree of alloying which reaches 11.0 at % in alloy 1421. On the other hand, scandium is used as a modifying agent in aluminium alloy 1421 to improve the set of mechanical properties, but the wider application of Sc is limited by its high price and small production volumes. However, Russia has sufficient scandium resources, as evidenced by the success of OK RUSAL in the production of scandium oxide with a purity level higher than 99% [47]. Therefore, the study of the properties of Al-based materials doped with Sc is an urgent task for material science.

The obtained results indicate that the study of the influence of the microstructure and the phase composition on the physical-mechanical properties of RS alloy 1421 is promising for optimization of its heat-treatment conditions, which are determined by the thermal stability of reinforcing phases. The established increase in the microhardness of foils upon their additional heat treatment is of practical interest for improving the technological processability of the alloy. The effect of the formation of the finely dispersed (Sc, Zr)-containing phase at temperatures around 300°C on the mechanical properties of foils requires additional studies, since this temperature meets the operating conditions at elevated temperatures and is close to the optimal temperature for obtaining bulk samples by compaction.

CONCLUSIONS

The performed studies show that the use of ultrafast quenching from the melt allows one to modify the microstructure of industrial aluminium alloy 1421 and obtain foils with a microcrystalline structure composed of a supersaturated solid solution. The inhomogeneous distribution of components over the RS alloy volume is established. The surface is enriched with lithium, whose content in the subsurface region of both sides of the foil is more than 17 times higher than the calculated concentration in the alloy. The annealing of foils at a temperature of 300°C for 1 h leads to the decay of the supersaturated solution and the precipitation of magnesium-containing and (Sc, Zr)-containing phases, the volume fractions of whose particles are 3.4 and 0.46 vol %, respectively. The specific surface areas of the interface boundaries for the precipitates of magnesium-containing and (Sc, Zr)-containing phases in the annealed foil are 0.51 and 0.40 μm^{-1}, respectively.

The microhardness of the rapidly solidified foils nonmonotonically changes during isochronal annealing, which is associated with the precipitation of metastable and stable phases in various temperature ranges. An increase in the microhardness of the foils in the temperature ranges of 50–100°C, 150–200°C, and 230–340°C is established. The presence of the precipitates of intermetallic phases, the size of which does not exceed 1 μm, leads to dispersion strengthening in the process of the annealing of alloy 1421 prepared by ultrafast crystallization and inhibits the recrystallization processes, thereby providing a plateau in the curve of the dependence of the microhardness on the isochronal annealing temperature in the temperature range of 340–400°C.

ACKNOWLEDGMENTS

We are grateful to S.V. Gusakova, leading engineer of the Intercollegiate Research Service Center of Belarusian State University, for her assistance in conducting the SEM and EDX experiments.

REFERENCES

1. I. N. Fridlyander, *Wrought Structural Aluminum Alloys* (Metallurgiya, Moscow, 1979) [in Russian].
2. I. N. Fridlyander, V. F. Shamrai, and N. V. Shiryaeva, Izv. Akad. Nauk SSSR, Met., **2,** 153–156 (1965)
3. N. I. Kolobnev, Met. Sci. Heat Treat. **44** (7–8), 297 (2002).

4. A. A. Mogucheva and R. O. Kaibyshev, Phys. Met. Metallogr., **106** (4), 424 (2008).
5. Yu. Buranova, V. Kulitskkiy, M. Peterlechner, A. Mogucheva, R. Kaibyshev, S. V. Divinski, and G. Wilde, Acta Materialia **124,** 210 (2017).
6. S. P. Yatsenko, L. A. Pasechnik, and V. M. Skachkov, Material Sci Technol News. **3,** 32 (2015).
7. Yu. M. Platov, L. I. Ivanov, V. T. Zabolotnyi, V. M. Lazorenko, and V. I. Tovtin, Non-Ferrous Met. (Moscow, Russ. Fed.), No. 10, 82 (2011).
8. A. P. Mukhachev, E. A. Kharitonova, and D. G. Skipochka, Vopr. At. Nauki Tekh., Ser.: Vak., Chist. Mater., Sverkhprovodn., No. 1, 45 (2016).
9. S. P. Yatsenko, G. M. Rubinshtein, and V. M. Skachkov, in *Proc. 5th Int. Res. and Appl. Sci. Conf., ExpoBuildRussia Spec. Forum* (UMTs UPI, Ekaterinburg, 2016), p. 75.
10. V. V. Zakharov V. I. Elagin, T. D. Rostova, and Yu. A. Filatov, Tekhnol. Legk. Splavov, No. **1**, 67 (2010).
11. Yu. D. Koryagin, M. A. Smirnov, S. S. Chernov, and N. T. Kareva, Vestnik YuUrGU, No. **34**, 58 (2010).
12. N. A. Belov, D. G. Eskin, and A. A. Aksenov, *Multicomponent Phase Diagrams: Applications for Commercial Aluminum Alloys* (Elsevier Science, Oxford, 2005).
13. V. G. Davydov, V. I. Elagin, V. V. Zakharov, and T. D. Rostova, Met. Sci. Heat Treat. **38** (8), 347 (1996).
14. Yu. A. Gorbunov, Engineering & Technologies, **5** (8), 636 (2015).
15. P. Yu. Kikin, A. I. Pchelintsev, E. E. Rusin, and N. V. Zemlyakova, Met. Sci. Heat Treat. **54** (7–8), 398 (2012).
16. I. P. Mishin, Nauchnoe obozrenie. Tekhnicheskie nauki, No. 2, 64 (2014).
17. A. Mogucheva and R. Kaibyshev, Metals, No. **6**, 254 (2016).
18. R. Kaibyshev, K. Shipilova, F. Musin, and Y. Motohashi, Mater. Sci. Technol **21** (4), 408 (2005).
19. A. M. Kuzei, *Structure and Phase Transformations in Fast-Quenched Aluminum Alloys* (Belaruskaya navuka, Minsk, 2011).
20. I. S. Miroshnichenko, *Liquid Quenching* (Metallurgiya, Moscow, 1982).
21. S. A. Saltykov, *Stereometric Metallography* (Metallurgiya, Moscow, 1976).
22. E. Schmidt, K. Ritter, K. Gartner, and E. Wendler, Nucl. Instrum. Methods Phys. Res. **409,** 126 (2017).
23. G. V. Vekilova, A. N. Ivanov, and Yu. D. Yagodkin, *Diffraction and Microscopy Methods and Instruments for Nanoparticle and Nanomaterial Analysis* (Izd. Dom MISiS, Moscow, 2009).
24. S. Hirosawa, T. Sato, A. Kamio, and H. M. Flower, Acta Mater. **48,** 1797 (2000).
25. L. Lochte, A. Gitt, G. Gottstein, and I. Hurtado, Acta Mater. **48,** 2969 (2000).
26. I. I. Tashlykova-Bushkevich, in *Proc. 12th Int. Conf. Aluminium Alloys (ICAA12)* (TMS, Yokohama, 2010).
27. I. Tashlykova-Bushkevich and G. Itoh, Mater. Sci. Forum **706–709,** 301 (2012).
28. P. Yu. Kikin, V. N. Perevezentsev, E. E. Rusin, and E. N. Razov, Fiz. Khim. Obrab. Mater., No. **1**, 18 (2012).
29. P. Yu. Kikin, V. N. Perevezentsev, E. E. Rusin, and E. N. Razov, Tech. Phys. **57** (2), 203 (2012).
30. V. V. Zakharov V. I. Elagin, S. G. Pavlenko, and T. D. Rostova, Fiz. Met. Metalloved., **60** (1), 97 (1985).
31. C. B. Fuller and D. N. Seidman, Acta Mater. **53** (20), 5415 (2005).
32. E. A. Lukina, A. A. Alekseev, V. V. Antipov, D. V. Zaitsev, and Yu. Yu. Klochkova, Russ. Metall. (Engl. Transl.), No. **6**, 60 (2009).
33. E. V. Naidenkin, Yu. R. Kolobov, E. V. Golosov, and I. P. Mishin, Phys. Mesomech., No. **9**, 133 (2006).
34. R. K. Islamgaliev, N. F. Yunusova, R. Z. Valiev, N. K. Tsenev, V. N. Perevezentsev., and T. G. Langdon, Scripta Mater. **49,** 467 (2003).
35. *Aluminum: Properties and Physical Metallurgy (Reference Book)*, Ed. by J. E. Hatch (Am. Soc. for Metals, Metals Park, Ohio (United States), 1984; Metallurgiya, Moscow, 1989).
36. N. I. Kolobnev, L. B. Khokhlatova, and E. Yu. Semenova, Metalloved. Tekhnol. Legkikh Splavov, No. **7**, 69 (1990).
37. M. I. Gol'dshtein, V. S. Litvinov, and B. M. Bronfin, *Metal Physics in High-Strength Alloys* (Metallurgiya, Moscow, 1986).
38. V. G. Shepelevich, Vestnik GGTU im. P.O. Sukhogo, No. **1**, 12 (2007).
39. S. V. Gusakova, M. Sukie, and V. G. Shepelevich, in *Collected Works 7th All-Russian Research Tech. Conf. with International Participation* (MATI, Moscow, 2008), p. 87.
40. G. -F. Yu, S. -Q. Zhang, Y. -S. Feng, and S. -C. Chai, Mater. Sci. Eng., A **133,** 274 (1991).
41. S. Ya. Betsofen, V. V. Antipov, and M. I. Knyazev, Russ. Metall. (Engl. Transl.), No. **4**, 326 (2009).
42. E. S. Gutko and V. G. Shepelevich, Fiz. Khim. Obrab. Mater., No. **4**, 81 (2005).
43. N. V. Zemlyakova and V. V. Kibitkin, Vestn. Tambov Univ. Ser. Nat. Tech. Sci. **21** (3), 1000 (2016).
44. P. A. Sivtsova and V. G. Shepelevich, in *Collected Works 7th All-Russian Research Tech. Conf. with International Participation* (MATI, Moscow, 2008), p. 10.
45. V. G. Shepelevich, Vestn. BGU. Ser. 1, Phys. Math. Computer Sci., No. **2**, 13 (2014).
46. N. K. Tsenev, V. N. Perevezentsev, M. Yu. Shcherban', and A. N. Tsenev, Tech Phys. **55,** 822 (2010).
47. I. N. Pyagay Non-Ferrous Met. (Moscow, Russ. Fed.), No. **7**, 43 (2016). 2016.

Translated by O. Kadkin